Mechanical Testing of FDM Parts for Process Simulation

Siddharth Dev, Prof. Christopher J. Hansen
(Department of Mechanical Engineering, University of Massachusetts at Lowell, Lowell MA, USA);

Blake Courter
(Stratasys Corp, Cambridge MA, USA);

Jing Bi, Vishal Savane
(Dassault Systemes Simulia Corp, Johnston RI, USA).

Abstract: *Fused Deposition Modeling (FDM) enables the development of functional prototypes, tooling, molds and fixtures of complex geometries which are difficult to manufacture using conventional manufacturing technologies such as injection molding. In the FDM process, thermoplastic materials such as ABS and ULTEM are extruded as filaments and deposited layer-by-layer to build a part directly from a CAD model. There are multiple factors in the FDM process that can affect the material properties of the final printed part. These include but are not limited to patterning direction, bead aspect ratio, air gap size and slice height. In order to perform accurate finite element process simulations, these FDM materials must be tested and characterized to measure primary mechanical properties against which the fidelity of simulation-driven material properties can be validated.*

In this study, the relationship between the layer-by-layer build process and the resulting mechanical properties is investigated. The build orientations are selected based on the assumption that the printed parts demonstrate orthotropic behavior, in which the properties will vary in the primary directions orthotropic to the build layer plane. This assumption is validated by mechanical testing of tensile and Iosipescu (shear) specimens fabricated with layer-by-layer orientations orthotropic to the loading axes. Properties that are obtained from the mechanical testing include tensile modulus, tensile strength, shear modulus and Poisson's ratio.

In addition to mechanical testing, virtual testing is also performed using a three-dimensional Representative Volume Element (RVE). The Abaqus micromechanics plugin is used to homogenize the linear elastic material constants. Periodic boundary conditions are used to represent the boundary effects of the microstructure formed during the printing process. Neither experimental nor virtual testing involves any empirical coefficients. The influence of the bead aspect ratio, bead volume fraction and geometry of the air gaps between the beads are investigated. A scaling factor is calculated to identify the correlation between the test material properties and simulation-driven *results. Good agreement is found between experimental and virtual testing. The testing results are readily usable for part-level FDM process simulation and in-service performance simulation.*

1. Introduction

Fused Deposition Modeling (FDM) is a popular layer additive manufacturing process used in many industries including aerospace, automotive, industrial, commercial and medical. Prototypes and end-use parts are produced by FDM from production grade thermoplastic materials such as ABS, polycarbonate and ULTEM. However, the in-service performance of FDM parts is highly dependent on the process parameters and residual stresses accumulated during printing. Many studies have been performed to characterize FDM printed materials and analyze the effect of process parameters. The characterization of FDM parts for rapid prototyping applications is a decades-old effort. Ahn et al. [1] studied raster orientation, air gap, bead width and other build parameters to quantify their effect on the final anisotropic material properties for ABS parts. Specimens with rasters oriented in line with the primary loading direction (i.e., 0º relative angle) demonstrate the highest tensile strength. A negative air gap results in an increased maximum tensile strength because the higher packing density of the rasters increases the specimen's load bearing ability. The typical FDM part exhibits a tensile strength that is 65-72% of an injection molded counterpart and a compressive strength that is 80-90% of an injection molded counterpart. In similar studies, Zeimian et al. [2] observed a significant effect of raster orientation on resulting polymer behaviour. Osborn et al. [3] studied the properties of FDM parts using both experimental and numerical approaches. A Representative Volume Element (RVE) is built using 6 by 4 bead widths; however, it is unclear how the periodic boundary condition was handled. Cantrell et al. [4] concludes that raster and build orientation had a negligible effect on Young's moduli and Poisson's ratio in ABS tensile specimens; by contrast, shear modulus and yield strength varied by up to 33%. Despite these research efforts, data from extensive experimental and numerical studies on a complete set of material behavior ready for use in process simulations is not readily available.

In this paper, we focus on the characterization and modeling of ABSplus P430 material coupons printed with a Stratasys Fortus 250mc machine. We start with experimental characterization of both injection molded and FDM printed materials. Orthotropic tensile moduli, Poisson's ratio and shear moduli are measured. Virtual characterization of FDM printed materials are also performed using a new multiscale micromechanics plugin developed in Abaqus/CAE. Injection molded material properties are used as intact deposition bead materials and RVE model of the microstructure is constructed with periodic boundary conditions based on analyses of microscope images. The experimental data are compared with results from an RVE homogenization model.

2. Experimental characterization of FDM printed parts

The mechanical properties of FDM printed parts are highly dependent on their raster orientations. The raster orientation is defined as the direction of the beads of material relative to the loading of the part [1]. FDM printed parts exhibit anisotropic behavior, and which are dependent on the choice of build parameters, such as raster orientation, bead width, air gap and slice height etc. [1,2,4]. Researchers have also attempted to characterize FDM printed coupons using CLT (Classical Laminate Theory), in which the coupon is assumed to be a laminate composed of orthotropic laminae. However, the CLT approach is only applicable to thin composite plates that demonstrate plane stress behavior, and therefore inaccurately represents the mechanical behavior of ‘thick’ FDM printed parts that possess thicknesses on the order of their transverse dimensions. In this research, the material constants for FDM printed parts are characterized under the assumption that they demonstrate orthotropic behavior with non-zero stresses in the out of plane direction. Unlike isotropic materials, orthotropic materials have different mechanical properties in three mutually perpendicular planes and can be characterized using nine engineering constants; three Young’s moduli, three shear moduli and three independent Poisson’s ratios. [5] These values can then be used to develop a stiffness matrix that correlates elastic stresses to their respective strains. This assumption of elastic behavior holds true for the process simulation analysis described in this paper because we only consider stress strain behavior in the elastic domain and do not expect high enough stresses that would extend into the plastic domain. We test FDM printed parts and determine their elastic moduli, shear moduli and Poisson’s ratios in accordance with this theory.

2.1 Materials and Fabrication

All FDM specimens were printed using red ABSplus-P430 material on a Stratasys Fortus 250mc machine. Rectangular coupon geometries with dimensions of 150 mm x 25.4 mm x 2.54 mm were first created in Solidworks® and then tessellated and exported in STL format to Stratasys’ Insight software. These STL files were then used to generate toolpaths for the layer by layer deposition process. Table 1 shows the print parameters used to manufacture all specimens. In this study, the slice height, raster width and air gap values were kept constant to ensure that the difference in values from testing could be directly correlated to print bed orientation rather than be influenced by machine parameters.

Table 1: Print Parameters for Coupon Testing

Parameter	Value
Slice Height	0.254 mm (0.010 in.)
Raster Width	0.406 mm (0.016 in.)
Air Gap	0

Rectangular coupons were printed following build orientations shown in Figure 1. The orientations of the beads/rasters can be visualized using Figure 2 which is a representation of each of these tensile specimens as though they were cut from a thick 3-D printed plate. The numbers beside each specimen in Figure 1 correspond to the numbers in Figure 2 for a corresponding macroscopic plate.

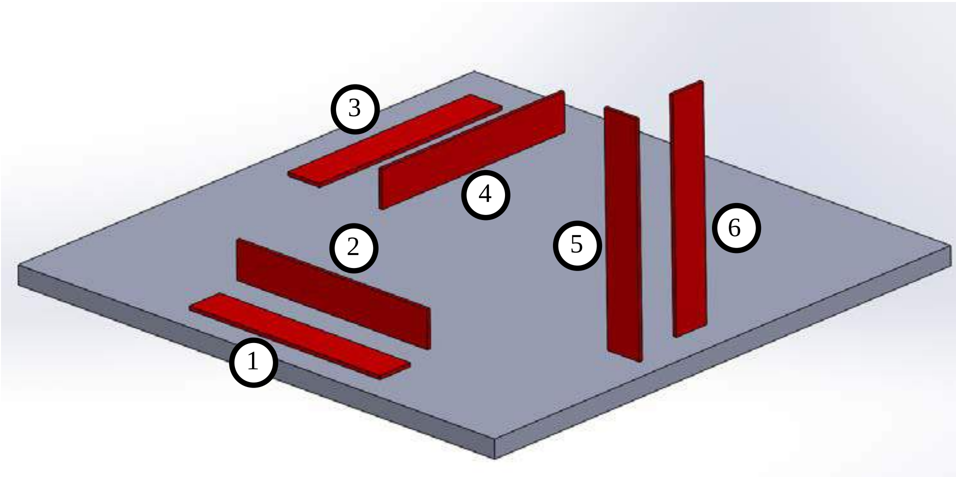

Figure 1: Print bed orientations for fabrication of FDM coupons

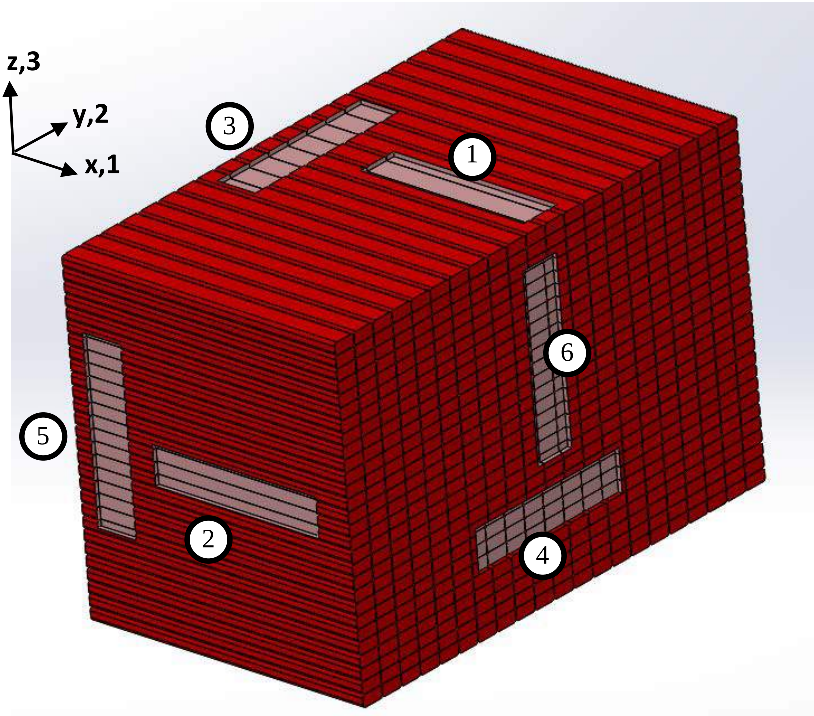

Figure 2: Orientations of all tensile specimens as if they were cut from a thick plate. Numbers correspond to specimens listed in Table 2.

In addition to FDM printed specimens, reference ABSplus-P430 injection molded dogbone specimens were manufactured and tested to determine isotropic properties for numerical simulation. Injection molded specimens were manufactured using an Engel CC90 injection molding machine with the parameters listed in Table 2.

Table 2: Injection Molding Parameters

Parameter	Value
Barrel Temperature*	200°C
Mold Temperature	32°C
Holding Pressure	8MPa
Holding Time	10 seconds
Back Pressure	2MPa
Injection Speed	51mm/sec

*Constant barrel temperature profile

2.2 Experimental Setup

The mechanical properties that were determined from the coupons printed in the various print bed orientations are provided in Table 3. The specimen numbers correspond to the numbers shown in Figures 1 and 2.

Table 3: Relationship between the print bed and mechanical global orientation systems

Specimen Number	Print Bed Orientation	Corresponding Elastic Modulus	Corresponding Poisson's Ratio	Corresponding Shear Modulus
1	XYZ	E_{11}	v_{12}	G_{12}
2	XZY	E_{11}	v_{13}	G_{13}
3	YXZ	E_{22}	v_{21}	G_{21}
4	YZX	E_{22}	v_{23}	G_{23}
5	ZXY	E_{33}	v_{31}	G_{31}
6	ZYX	E_{33}	v_{32}	G_{32}

All rectangular FDM specimens and dogbone injection molded specimens were tested following specifications in ASTM D3039 and ASTM D638, respectively. Specimens were clamped using mechanical wedge action grips and subsequently tested on a load frame (Instron 3367) with a 30 kN load cell. For tensile tests, axial and transverse strains were obtained using bi-axial strain gages (Omega Engineering-SGT-4/350-XY13) wired to electrical adapters compatible with the Instron 3300 series. For FDM specimens, shear moduli were obtained following test specifications in ASTM D5379 (Iosipescu Shear). Strain data required for shear modulus calculations was obtained from 45 degree rosette strain gages (Omega Engineering-SGT-2D/350M-SY1) that were attached to one face of the Iosipescu specimens. All data was recorded using Instron's Bluehill 3 software and data analysis was performed using Microsoft Excel.

2.3 Characterization of Bead Shape and Volume Fraction

The fracture surface of ABS specimens was imaged using an optical microscope to determine the representative bead shape and bead volume fraction in the tested specimens. The averaged width (w_{touch}) and height (h_{touch}) of the contact regions of 18 beads in the microscopic image were obtained using ImageJ software. These values were then used to create a representative bead shape (Figure 3) that is used for subsequent simulation testing. In addition to bead shape, the bead volume fraction was obtained by applying a Shanbhag threshold to the microscope image.

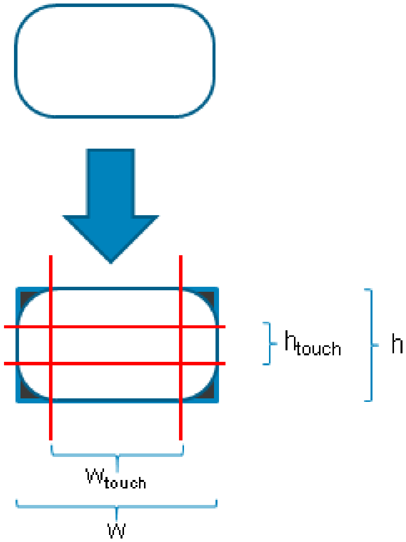

Figure 3: Bead shape is assumed to be a rounded rectangle based on information processed from microscope images.

2.4 Experimental results

Isotropic data for injection molded ABSplus-P430 specimens is summarized in Table 4. Shear modulus was calculated using Equation 1.

$$G = \frac{E}{1 + 2v} \qquad \text{Eqn. 1}$$

Table 4: Isotropic moduli of injection molded ABS-plus P430 from experimental testing

Description	Tensile Moduli (GPa)	Shear Moduli (GPa)	Poisson's Ratio
	E	***G***	***v***
Average	2.8025	1.6789	0.335
Std Dev	0.0290	0.0339	0.0265
Error (%)	1.0342	2.0215	7.8978

Three specimens were printed for each combination of build and raster orientation listed in Table 3. Eighteen tensile specimens were tested in total; Figure 4 shows representative failure modes of the tested specimens.

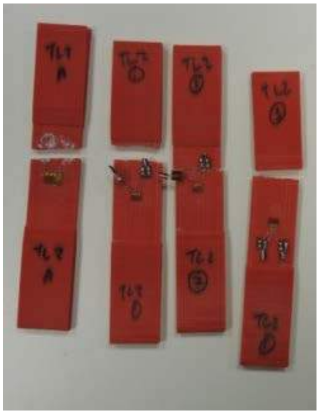

Figure 4: Post-test ABS specimens showing failure occurred in the gage length

A summary of the elastic moduli and Poisson's ratios that were obtained from tensile testing are shown in Table 5. Two values were obtained for E_{11}, E_{22} and E_{33} each based on the orientations listed in Table 3.

Table 5: Linear elastic moduli and Poisson's ratios for red 3-D printed ABSplus-P430

Description	Tensile Moduli (*GPa*)						Poisson's Ratio		
Specimen Number	**1**	**2**	**3**	**4**	**5**	**6**	**1 (2)**	**3 (5)**	**4 (6)**
Material Property	E_{11}	E_{11}	E_{22}	E_{22}	E_{33}	E_{33}	$\nu_{12}\ (\nu_{13})$	$\nu_{21}(\nu_{31})$	$\nu_{23}(\nu_{32})$
Averaged Values	2.47	2.44	1.95	2.70	2.13	2.60	0.34(0.32)	0.31(0.32)	0.36(0.37)
Std. Dev	0.08	0.12	0.03	0.19	0.09	0.14	0.01(0.02)	0.02(0.03)	0.01(0.03)
% Uncertainty	3.19	4.87	1.64	6.96	4.55	5.29	3.84(4.72)	7.90(10.2)	3.29(8.00)

The data corroborates the initial hypothesis that a 3-D printed FDM part is not isotropic in nature. In addition, the coupons exhibit the greatest stiffness in the *11*-direction (i.e., 0º raster orientation) with the elastic modulus approximately 15-20% greater than those in the transverse orientations. The elastic modulus in the *33*-direction is higher than the modulus in the *22*-direction by 9%. This is likely due to the fact that the contact area between the rounded rectangular beads is greater in the z-direction than in the y-direction.

A more detailed observation of the moduli shows that, while the values for specimens 1,3 and 5 conform to expectation of how an orthotropic material should behave, the build orientations for the E_{22} and E_{33} specimens had a significant impact on their respective directional moduli. This behavior can again be attributed to the impact of a high raster volume fraction per unit area and increased bead compaction for specimens 4 and 6 when compared to specimens 3 and 5 respectively. For E_{22}, specimen 3 and 4 show a 40% difference in value while for E_{33}, specimen 5 and 6 show a 22% difference in value. Further testing will be conducted on a larger number of specimens to reduce the uncertainty for the individual moduli values.

In orthotropic materials, the Maxwell-Betti reciprocal theorem can be used to validate the accuracy of the tested data as well as to verify if the theory of orthotropic behavior holds true [7]. Equations 2, 3 and 4 must hold true if orthotropic agreement exists between the linear elastic material constants.

$$\frac{\nu_{12}}{E_{11}} = \frac{\nu_{21}}{E_{22}} \qquad \text{Eqn. 2}$$

$$\frac{\nu_{13}}{E_{11}} = \frac{\nu_{31}}{E_{33}} \qquad \text{Eqn. 3}$$

$$\frac{\nu_{23}}{E_{22}} = \frac{\nu_{32}}{E_{33}} \qquad \text{Eqn. 4}$$

Based on the data reported in Table 5, the average values for the pairs of specimens used to calculate E_{11}, E_{22} and E_{33} are chosen to be substituted into the Maxwell-Betti equations. Table 6 shows a summary of the values calculated using Equations 1-3. While the low percent error indicates that this material shows excellent orthotropic agreement, further studies will be conducted to determine if the assumption remains true for other build structures.

Table 6: Equivalent properties for FDM printed coupons under assumption of Maxwell-Betti reciprocity

Property Relationship	$\frac{\nu_{12}}{E_{11}}$	$\frac{\nu_{21}}{E_{22}}$	$\frac{\nu_{13}}{E_{11}}$	$\frac{\nu_{31}}{E_{33}}$	$\frac{\nu_{23}}{E_{22}}$	$\frac{\nu_{32}}{E_{33}}$
Value	0.138	0.135	0.140	0.135	0.158	0.164
% Difference Between Values	1.21		2.58		2.73	

3 Virtual Characterization of FDM Printed Parts

The Abaqus multiscale micromechanics plugin (Figure 5) was developed in Abaqus 2017. This is an Abaqus/CAE plugin and includes helpful functionalities for setting up and post-processing FE-RVE models [8]. Model setup includes the imposition of far-field loading through periodic or non-periodic boundary conditions, and setting up the loads and analysis steps necessary to perform homogenization of properties. Post processing includes determining the homogenized properties of the FE-RVE from the completed analysis as well as performing averaging and statistical analysis of the fields in the whole RVE and within individual RVE constituents. Mechanical, thermal, coupled temperature-displacement as well as solid-to-shell homogenization options are available.

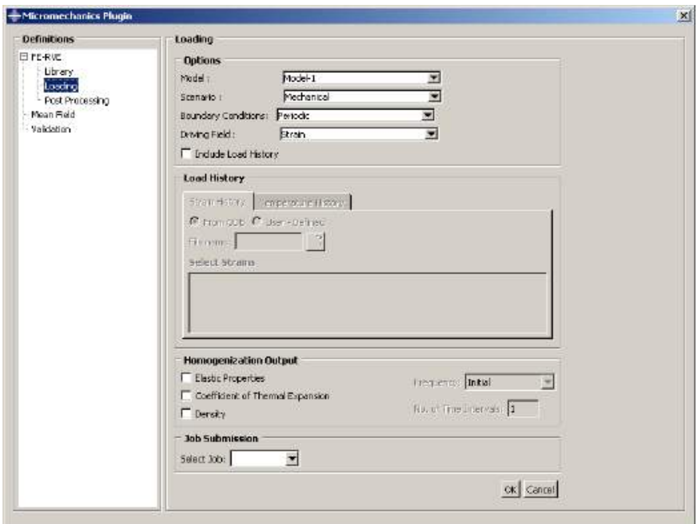

Figure 5: Abaqus/CAE micromechanics plugin interface

There are a broad variety of applications and workflows that these capabilities can be applied to. Some of the plugin's functionalities include the ability to; 1) handle voids, 2) understand bonding behavior and 3) simulate multiple materials. This versatility enables the plugin to be used for virtual testing and characterization of FDM printed parts. The rest of this section will present in detail the assumptions, parameters and homogenization workflow with periodicity considered.

Based on observation of the micro scanned images of the cross section of the FDM parts, it is assumed that the bead cross section is of a rectangular shape but with four circular shaped corners as shown in Figure 6. Bead volume fraction is calculated as 96% by measuring the total area of the cross section and the total area of the beads. Bead aspect ratio (width to height ratio) is determined by averaging the values of 18 beads and the parameter *w/h* is calculated to be 2. The RVE model was generated in Abaqus/CAE with the cross-sectional shape and dimensions shown in Figure 6. Periodic boundary conditions are applied automatically in the micromechanics plugin using the equation constraint. The micromechanics plugin includes internal algorithms for handling inconsistent nodal positions at opposite faces where periodic boundary condition is prescribed. Therefore, there is no restriction on the mesh consistency on opposite faces for the RVE model. The linear material homogenization option is used to obtain the elastic moduli and constants. Six perturbation load cases are generated by the micromechanics plugin each of which includes a unit strain loading applied to the RVE reference point. The plugin post processes the results from the perturbation load cases and calculates the homogenized material stiffness matrix and engineering constants.

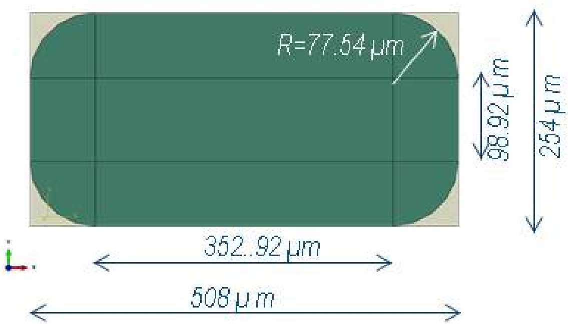

Figure 6: Cross section and dimension of the RVE model in Abaqus/CAE

The injection molded ABSplus-P430 properties are applied as the bead material properties. Table 4 shows the averaged isotropic moduli from 4 repeated test samples. The void is either left empty or can be modelled with elements applied with negligible properties and in this paper we choose the latter. Figure 7 shows the deformed shape of the RVE model under six perturbation load cases including unit tensile strain in *x*, *y*, *z*, and unit shear strain in *xy*, *xz* and *yz*. The results are post processed by the plugin and a stiffness matrix or engineering constants are obtained.

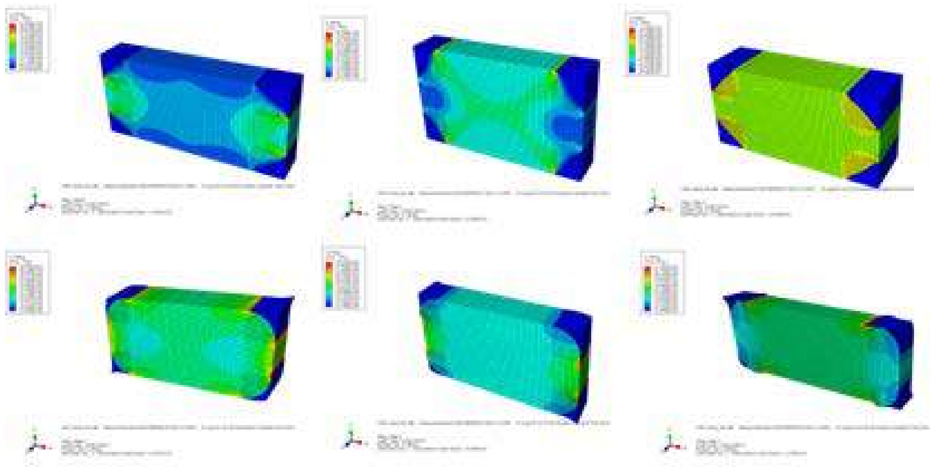

Figure 7: Virtual testing using Abaqus micromechanics plugin

The orthotropic tensile moduli of FDM ABS-plus P430 from experimental testing as well as RVE homogenization are provided in Table 7 and Table 8, respectively. Table 8 shows that the difference in value of the moduli between the experimental and RVE values. The maximum difference, at 9%, is low. It must be noted, however, that the experimental data selected for comparison to the simulation data only takes into account the moduli for specimens 1, 3 and 5 from Table 2. This data usage is because RVE homogenization is performed on a microstructure based on averaged bead aspect ratio and void fraction from the SEM image of a single tensile specimen. The moduli obtained from specimens 1, 3 and 5 have a bead microstructure that matches the RVE model most accurately.

Table 7:Orthortropic Tensile Moduli of FDM ABSplus-P430 from experimental testing

Description	E_{11} (*GPa*)	E_{22} (*GPa*)	E_{33} (*GPa*)
Average	2.47	1.95	2.13
Std Dev	0.08	0.03	0.09
Scatter (%)	3.19	1.64	4.55

Table 8: Orthotropic Tensile Moduli of FDM ABSplus-P430 from RVE Homogenization

Description	E_{11} (GPa)	E_{22} (GPa)	E_{33} (GPa)
Value	2.69	2.13	2.26
Variation from experimental data (%)	8.91	9.23	6.10

Table 9 shows all other engineering constants predicted by the micromechanics plugin. The shear moduli are predicted as being reasonably close to the values obtained from experimental testing. G_{23} shows higher difference when compared to experimental average (14.8%). However, experimental testing for G_{23} also shows a greater scatter between specimens (9.6%). The Poisson's ratio prediction shows a 22% max difference to experimental result, a larger value when compared to experimental scatter (a maximum of 10% standard deviation) The experimental scatter can be due to the variation in the microstructures of individual coupons. The difference as compared to experimental measure arises from the averaged assumption of void fraction and bead shape. It is expected that if the number of test coupons increases, or if the RVE model assumptions are based on a larger number of beads and more microscope images, the difference between both approaches will decrease. The addition of bead bonding to the model may also improve the fidelity of the RVE homogenization.

Table 9: All other engineering moduli of FDM ABSplus-P430 from RVE homogenization

Description	v_{12}	v_{13}	v_{23}
Value	0.2653	0.2818	0.3037
Description	G_{12} (GPa)	G_{13} (GPa)	G_{23} (GPa)
Value	0.8942	0.9167	0.8951

4 Discussion

It can be seen from both experimental and virtual characterizations that FDM printed part properties are highly dependent on the process parameters and bead microstructure. The material deposition flow direction (1-direction) is the strongest. The other two directions are weaker in comparison to the in-plane direction with the 2-direction being the weakest due to the fact that 2-direction has the smallest bond to void area ratio. This phenomenon is a direct result of the bead geometry's aspect ratio ($w/h = 2$) chosen for this analysis.

Knock down factors are defined as the ratio of either the experimental value or the RVE prediction of the moduli to the injection molded moduli. The knock down factors for experimental data and

RVE data are listed in Table 10. It is found that shear moduli are affected more by the FDM process. RVE results show more variation in directional Young's moduli than the experimental results and this could be attributed to the absence of a model that simulates bead bonding in the RVE.

Table 10: Knock down factors from injection molded ABSplus-P430

	E_{11}	E_{22}	E_{33}
Experiment	0.875	0.696	0.761
RVE	0.960	0.760	0.807
	v_{12}	v_{13}	v_{23}
Experiment	1.01	0.94	1.104
RVE	0.792	0.841	0.907
	G_{12}	G_{13}	G_{23}
Experiment	0.596	0.524	0.625
RVE	0.533	0.546	0.533

Parametric studies of the process parameters can be very useful for obtaining insight into how each parameter affects the properties of the printed part. The micromechanics plugin can be easily used to investigate the influence of different direct/indirect process parameters such as the bead aspect ratio, void fraction, slice height and geometry of the air gaps between the beads. In this virtual testing section, we have performed parametric studies on the bead aspect ratio and void fraction.

Table 11 shows the change in each engineering constant with bead aspect ratio varying from 1 to 3. The slice height (254 μm) and void fraction (96%) are kept constant. It can be seen from Table 10 that the change in E_{22} with increasing bead width is in opposite direction as those of E_{11} and E_{33}. Opposite trends are also seen for shear moduli and Poisson's ratio. Table 12 shows the RVE predicted knock down factors from injection molded ABS coupons. Shear moduli are knocked down significantly more than other moduli.

Table 11: Mechanical moduli characterized by RVE virtual testing

Bead Aspect Ratio	E_{11} (MPa)	E_{22} (MPa)	E_{33} (MPa)	v_{12}	v_{13}	v_{23}	G_{12} (MPa)	G_{13} (MPa)	G_{23} (MPa)
1	2688	2183.1	2194.8	0.27	0.27	0.33	910	911	912
1.5	2689	2159.6	2217	0.27	0.28	0.32	902	913	904
2	2689	2129.9	2262.9	0.27	0.28	0.30	894	917	895
2.5	2689.7	2116.3	2291	0.26	0.29	0.29	886	919	886
3	2689.8	2090.9	2321.6	0.26	0.29	0.28	876	922	876

Table 12: RVE predicted knock down factors from injection molded ABS coupons

Bead Aspect Ratio	E_{11} (MPa)	E_{22} (MPa)	E_{33} (MPa)	v_{12}	v_{13}	v_{23}	G_{12} (MPa)	G_{13} (MPa)	G_{23} (MPa)
1	0.96	0.78	0.78	0.81	0.82	0.97	0.54	0.54	0.54
1.5	0.96	0.77	0.79	0.80	0.82	0.94	0.54	0.54	0.54
2	0.96	0.76	0.81	0.79	0.84	0.91	0.53	0.55	0.53
2.5	0.96	0.76	0.82	0.79	0.85	0.88	0.53	0.55	0.53
3	0.96	0.75	0.83	0.78	0.86	0.85	0.52	0.55	0.52

5 Conclusion and Future Work

Experimental and virtual characterizations were performed for ABSplus-P430 parts printed using the Stratasys Fortus 250mc machine. Injection molded coupons were also experimentally tested to provide a basis for the RVE homogenization. RVE predictions and experimental results are closely matched but further investigated is warranted to determine the impact of variations in bead shape and volume fraction on the predicted properties. Parametric studies were performed using virtual characterization with RVE. The effect of different aspect ratios was investigated. Different trends were found between different directional moduli.

RVE prediction shows that the Young's moduli of FDM printed parts reduces by 4% to 25% in comparison to injection molded parts depending on the direction that is considered. Larger dependence on direction was observed in RVE prediction than in experimental tests, which could be due to the lack of a robust modeling strategy for the bonding between beads. It was found that shear moduli decreased the most, and only demonstrated a maximum value of between 52% and 62% of injection molded parts.

Further research will be performed to characterize the temperature dependency on the mechanical as well as thermal properties of an FDM printed ABS part. Properties that will be investigated include temperature dependent mechanical moduli, thermal conductivity, coefficient of thermal expansion and specific heat. This will enable complete characterization of the material for FDM process simulation [5]. DMA testing will be used to study how the mechanical moduli reduce as the temperature is increased up to melting temperature while TMA testing will provide information on how the coefficient of thermal expansion varies with increasing temperature. Both are critical to being able to develop an effective process simulation tool because they have a direct impact on part distortion during the FDM process. The values obtained for the thermal expansion coefficient, thermal conductivity and specific heat capacity can then be compared with results from RVE homogenization.

6 References

[1] Ahn, S. H., Montero, M., Odell, D., Roundy, S. and Wright, P. K. (2002). Anisotropic material properties of fused deposition modelling ABS. Rapid prototyping Journal, 2002, 8(4), 248-257.

[2] Ziemian, C., Sharma, M., Ziemian, S., (2012) Anisotropic Mechanical Properties of ABS Parts Fabricated by Fused Deposition Modeling, Mechanical Engineering, Dr. Murat Gokcek (Ed.), ISBN: 978-953-51-0505-3.

[3] Osborn, T., Zhou, E. Gerzeski, R., Mollenhauer, D., Tandon, G. P., Whitney, T. J., and Iarve, E. V. (2015). Proceedings of the American Society for Composites.

[4] Cantrell, J., Rohde, S., Damiani, D., Gurnani, R., DiSandro, L., Anton, J., Young, A., Jerez, A., Steinbach, D., Kroese, C. and Ifju, P. (2017). Experimental Characterization of the Mechanical Properties of 3D Printed ABS and Polycarbonate Parts. Proceedings of the Society for Experimental Mechanics Series, September 8, 2016.

[5] Nettles, Alan T. "Basic mechanics of laminated composite plates." (1994).

[6] Courter, B., Savane, V., Bi, J., Dev, S. and Hansen, C. J. (2017). Finite Element Simulation of the Fused Deposition Modelling Process. Proceedings of the NAFEMS World Congress 2017, Stockholm, Sweden, June 11-14.

[7] Hyer, Michael W. Stress analysis of fiber-reinforced composite materials. DEStech Publications, Inc, 2009.

[8] Micromechanics Plugin for Abaqus/CAE, Abaqus Documentation, Abaqus 2017, Dassault Systèmes Simulia Corp., 2017.